On-Demand Magnetically-Activated Drug Delivery from Additively Manufactured Porous Bone Implants to Tackle Antibiotic-Resistant Infections

Šalandová, Monika; Leeflang, Marius Alexander; Klimopoulou, Maria; Fratila-Apachitei, Lidy Elena; Apachitei, Iulian; Zadpoor, Amir Abbas

DOI
10.1002/admt.202301616

Publication date
2024

Document Version
Final published version

Published in
Advanced Materials Technologies

ADVANCED MATERIALS TECHNOLOGIES
www.advmattechnol.de

On-Demand Magnetically-Activated Drug Delivery from Additively Manufactured Porous Bone Implants to Tackle Antibiotic-Resistant Infections

Monika Šalandová, Marius Alexander Leeflang, Maria Klimopoulou, Lidy Elena Fratila-Apachitei, Iulian Apachitei,* and Amir Abbas Zadpoor*

This study proposes a new concept for an on-demand drug releasing device intended for integration into additively manufactured (i.e., 3D printed) orthopedic implants. The system comprises a surface with conduits connected to a subsurface reservoir used for storage and on-demand release of antimicrobial agents, covered with a cap that prevents the antibacterial agents from being released until alternating magnetic field (AMF) raises the temperature of the cap, thus, releasing the stored drug. To demonstrate this concept, Ti6Al4V specimens are directly 3D printed using selective laser melting and their surface, reservoirs, and drug releasing properties are characterized. A new synthetic antimicrobial peptide, SAAP-148, is thereafter tested for its cytotoxic, osteogenic, and immunomodulatory effects at concentrations relevant for its minimal bactericidal concentration (MBC) and is compared with its natural analogue, LL-37. The results showed that AMF successfully activated the release from the 3D printed loaded samples. Both peptides demonstrated to be non-cytotoxic within the MBC levels for macrophages and preosteoblasts and did not influence their osteoimmunomodulatory behavior. The findings of this study indicate that the proposed concept is technically feasible and has the potential to be used for the development of bone implants with on-demand delivery systems to fight IAI without systemic or continuous local release of antibiotics.

1. Introduction

Mature bacterial biofilms on biomaterials present a major treatment challenge in clinics, often requiring surgical debridement and (two-stage) revision surgeries alongside systemic administration of antibiotics.[1–3] In orthopedics, implant-associated infection (IAI) is still one of the major complications following the surgery, possibly leading to a failure of an implant.[4] While it affects approximately 1%–2% of patients undergoing a primary total hip arthroplasty,[5–7] there is a 5–10-fold rise in infection likelihood following revision surgeries,[8] and a generally greater susceptibility in patient groups suffering from immune deficiencies or other comorbidities.[9,10]

For decades now, (mostly systemically administered) antibiotics have played a predominant role in the prevention and treatment of IAIs.[4,6] Their future is, however, accompanied by a great uncertainty due to the growing number of bacteria which have succeeded to survive, adapt, and eventually also thrive in such presumably hostile environments.[11,12] Nowadays, such resistant organisms are increasingly found not only in IAI but in all acquired infections.[13] In isolates from infected biomaterials, the highest occurrence rates of resistant phenotypes are registered with some gram-negative strains (20%–40%),[9] and include the notorious methicillin-resistant *Staphylococcus aureus* (MRSA).[6,14]

Due to the uncertain future role of antibiotics in IAI, there has been a move toward the development of antibacterial biomaterials endowed with local-action mechanisms and the possibility to prevent IAIs in the first place. Direct antibacterial biomaterials intended for orthopedic applications can be divided into three major categories: anti-adhesive/repelling surfaces, contact killing surfaces, and antibacterial-leaching surfaces, each of them exhibiting varying pros and cons.[15] Antiadhesive surfaces do not represent a suitable choice for orthopedics as they often impede the adhesion of host cells as well, nonetheless, they show success in solutions where cell adhesion is undesirable in general, such as biomaterials for catheters. Contact killing can manifest greater selectivity toward bacterial cells, however, once the surface is

M. Šalandová, M. A. Leeflang, M. Klimopoulou, L. E. Fratila-Apachitei, I. Apachitei, A. A. Zadpoor
Department of Biomechanical Engineering
Faculty of Mechanical Engineering
Delft University of Technology
Mekelweg 2, Delft 2628 CD, Netherlands
E-mail: m.salandova@tudelft.nl; i.apachitei@tudelft.nl
A. A. Zadpoor
Department of Orthopedics
Leiden University Medical Center
Albinusdreef 2, Leiden 2333 ZA, Netherlands

The ORCID identification number(s) for the author(s) of this article can be found under https://doi.org/10.1002/admt.202301616

DOI: 10.1002/admt.202301616

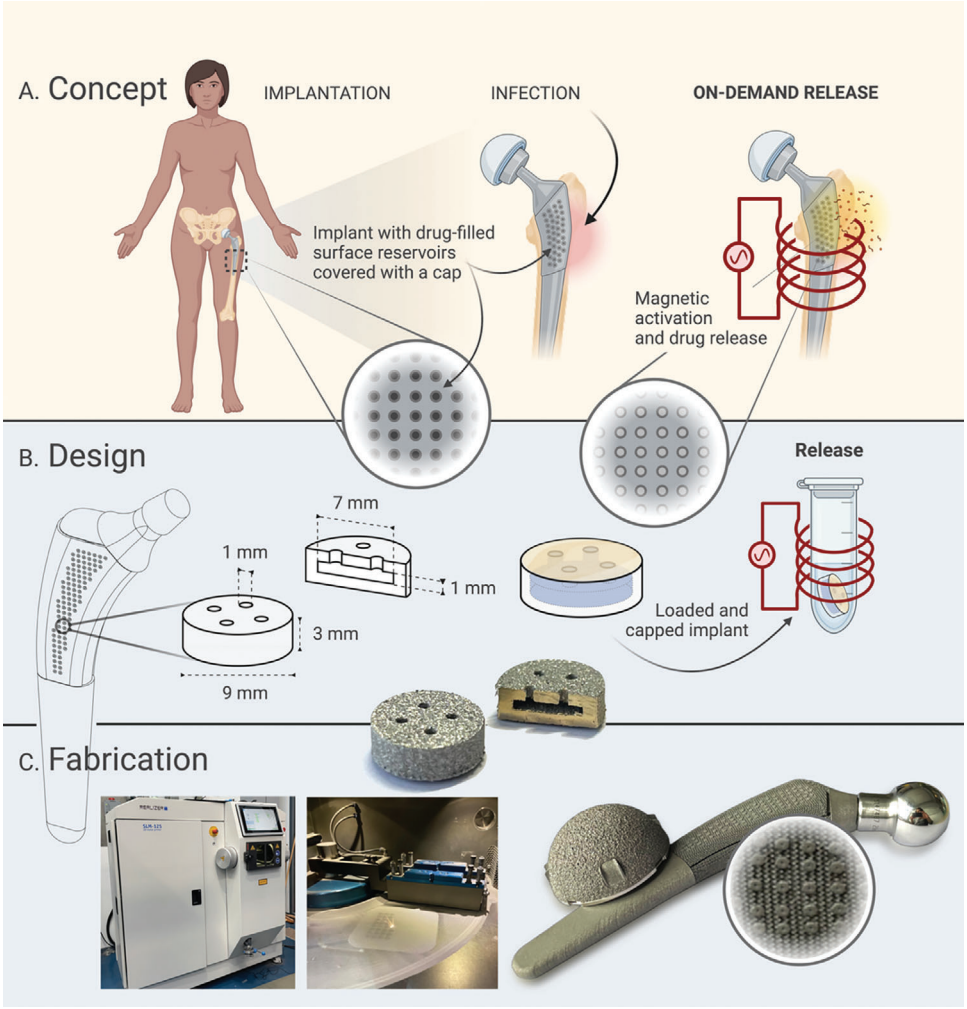

Figure 1. A) Concept: A local on-demand drug delivery system was designed to release the drug upon exposure to an alternating magnetic field in an event of implant-associated infection; B) Design: As a proof-of-concept, specimens representing a small unit of the implant with reservoirs were designed and tested in a release experiment; C) Fabrication: A laser powder bed fusion additive manufacturing process (i.e., selective laser melting) was used to fabricate the specimens and the real-size implant. Created with BioRender.com.

covered, the effect may be reduced or lost, unless it can be recovered (i.e., under flow conditions or due to phagocytosis).[16] Additionally, both of those approaches target adherent bacteria and lack any capacity to eliminate planktonic cells. Antibacterial-releasing biomaterials dispense the drug into the surroundings from the surface/bulk material as a result of various processes (diffusion, hydrolysis, degradation)[15,17] and are able to target both planktonic and adherent bacteria. With time, however, the long-sustained release of those coatings becomes their major weakness, as the drug gradually depletes and the levels eventually drop below the therapeutic bactericidal dose, which introduces risks of further contributing to the spread of resistant organisms.

To overcome the risks represented by antimicrobial resistance (AMR), the field has recently started shifting its focus toward the next generation of antibacterial biomaterials, emphasizing precision, and gaining control over the delivery of a drug with low propensity to induce resistance. Within the backdrop of such developments, we are proposing here the novel concept of on-demand local drug delivery from additively manufactured orthopedic biomaterials, where the release of antibacterial agents can be activated remotely upon infection detection. Such configuration (**Figure 1A**) could reduce the need for systemic administration of antibiotics, thereby limiting the rise of AMR while also protecting patients from the adverse effects of such treatments.[18] Moreover, the on-demand delivery of antibacterial agents from the reservoirs incorporated into the implant enables us to maintain therapeutic levels during the treatment instead of continuously delivering antibacterial agents from the implant, which would eventually lead to prolonged sub-therapeutic concentrations.

Here we use antimicrobial peptides (AMPs) instead of antibiotics,[3] or metallic ions,[19] as they have shown to possess the ability to withstand repeated exposures without eliciting bacterial resistance,[20,21] and to be less likely than metallic ions to cause cytotoxicity.[22] In fact, they have attracted attention for their selectivity toward bacteria,[23,24] capacity to target the strains that are the usual culprits in IAIs,[25] and ability to prevent biofilm formation.[20,26] As immunomodulatory agents, they can steer

the immune system, thereby strengthening its pathogen-clearing ability and, at the same time, aiding tissue regeneration by promoting angiogenesis as well as attracting and modulating immune and other cells involved in the healing process.[27–29] Despite their advantages, some AMPs may instigate undesirable and adverse responses due to their cytotoxicity at high concentrations or interference in various physiological processes.[30] Therefore, they must be used with care and their effects must be adequately monitored.

In this concept, the 3D printed Ti6Al4V orthopedic implants are equipped with reservoirs whose contents (i.e., AMPs) are released on-demand upon activation by magnetic fields. The implant is additively manufactured through selective laser melting to incorporate reservoirs that are capped by poly(lactic-co-glycolic acid) (PLGA) films. Upon exposure to alternating magnetic field (AMF) and generation of eddy currents, a temperature-dependent mechanism leads to the release of the drug present in the reservoirs. We study the on-demand release kinetics of a model molecule while also investigating the performance of two AMPs, a synthetic SAAP-148 and its natural analogue, LL-37, in terms of their cytotoxicity as well as their immunomodulatory and osteogenic properties in vitro, for potential incorporation into the proposed system.

2. Experimental Section

2.1. Rational Design of Implants Incorporating On-Demand Delivery Systems

To enable the storage and local release of an antimicrobial drug, samples with interconnected surface reservoirs were designed (Figure 1B) in two configurations with 4 and 5 reservoir conduits (1.0 mm in diameter, 1.0 mm high). The overall dimensions of the sample (9.0 mm in diameter, 3.0 mm high) were chosen to comply with the geometrical constraints of cell-culturing well plates. The conduits were connected to a reservoir (7.0 mm in diameter, 1.0 mm high) to maximize the utilization of the sample volume for drug storage and to enable the control and reproducibility of drug loading. The surface reservoirs could be loaded by using a Luer-Lock syringe and a 22 Gauge metal nozzle. The theoretical volume of the reservoirs was 41.6 and 42.4 mm^3, and the ratio of the conduits to the surface area was calculated to be 1:19 and 1:15 for the four- and five-reservoir configurations, respectively. Figure 1C also captures the envisioned integration of the reservoirs into hip implants. The reservoirs were accommodated at the proximal area of the stem of the implant, which is a crucial interface for attachment of uncemented implants and distribution of physiological load.[31] The size and distribution of the reservoirs may be adjusted based on the release kinetics of the drug and the geometry of the actual implant.

2.2. Additive Manufacturing

The specimens were fabricated through selective laser melting (SLM), which is a laser-based powder bed fusion (PBF) additive manufacturing technique. The fabrication was completed on a SLM machine (SLM-125 Realizer, Borchen, Germany) (Figure 1C). Medical grade 23 Ti6Al4V alloy (with extra low interstitials) was selected and used in the form of spherical powder (AP&C, Boisbriand, Quebec, Canada) with particles sizes in the range of 10–45 µm. The SLM equipment used Ytterbium laser (400 W, 5000 mA at full capacity). The alternating scanning strategy was set to 90°. While fixing the laser current and scanning time to 1100 mA and 20 µs, respectively, we varied the hatching distance to study its effects on the porosity of the printed specimens (90, 105, 120, 150 µm). The aim was to identify the optimal hatching distance to achieve a high density of the printed material to ensure, on the one hand, that the drug did not leak out of the reservoir and that high mechanical properties were achieved while, on the other hand, preventing the undesired defects of overheating. The samples were then vacuum cleaned, sonicated in isopropanol and water (both for 5 min), and air dried.

2.3. Morphological Characterization

The surface morphology of the printed samples was characterized using scanning electron microscopy (SEM, JSM-IT100, JEOL, Tokyo, Japan). A vertical cross-sectional analysis was performed to confirm the cleaning efficiency and the printing accuracy of the inner features. Quantitative analysis of the surface roughness and the inner geometry was carried out using a Profilm3D optical profilometer (Filmetrics, San Diego, California, USA). Arithmetic average area roughness was chosen in this study instead of line roughness due to the inhomogeneity of the surface. A Gaussian filter (Spline Gaussian $\beta = 0.625242$, $\lambda_c =$ 120 µm) was applied and the surface roughness was calculated according to ISO 25178 in the software accompanying the profilometer.

2.4. On-Demand Release

To demonstrate the proposed concept, the loading and on-demand release of a model molecule mixed in hydrogel were studied. The surface was covered with a PLGA film to prevent the release of the model molecule from the conduits. An AMF triggered the release of the model molecule due to the heat generated by the eddy current in the Ti6Al4V specimen, which led to the disruption of the PLGA film and, thus, on-demand release of the incorporated drug. The workflow is illustrated in **Figure 3A** together with the results.

To incorporate the model molecule into a hydrogel, ultrapure low viscosity alginate (PRONOVA UP LVG Alginate, DuPont Nutrition Norge AS, Sandvika, Norway) was dissolved in 0.9% NaCl to final concentration of 5 w/w% of sodium alginate and stirred until homogeneous. Blue food dye (Trend Decor B.V., Boekel, the Netherlands) was used as a model molecule and mixed with the hydrogel. Hydrogel was then loaded into the samples through one of the conduits using 1 ml Luer-Lock syringes combined with a 22 Gauge metal nozzle.

To fabricate the PLGA caps, Resomer RG 504 H Poly(D,L-lactide-co-glycolide) (Sigma Aldrich, Zwijndrecht, The Netherlands) was dissolved in acetone to a final concentration of 10 w/w%. A volume of 80 µl of the solution was then pipetted on parafilm-covered glass slides and left to dry for at least 1 h to produce thin films.

The films were then peeled off and pressed onto the loaded Ti6Al4V samples to cover the reservoir conduits (experimental groups PLGA-37 and PLGA-AMF75). For control samples, the loaded specimens were left without the PLGA films (noPLGA-37).

The samples were transferred into 2 ml Eppendorf tubes containing 700 μl of demineralized water and were placed in a water bath set to 37 °C for 5 h. The absorbance of the supernatant was then measured on a VICTOR X3 Multilabel Plate Reader (PerkinElmer Nederland B.V., Groningen, The Netherlands) at 656 nm. After the reading, one group of the specimens with the PLGA films was placed in a MagneTherm, an alternating magnetic field setup, (NanoTherics Ltd., Warrington, United Kingdom) for 30 min to trigger the release (PLGA-AMF75). The AMF exposure was carried out at a frequency of 262 kHz and a field strength of 5 mT. Temperature was monitored with two fiber optic probes immersed in the solution surrounding the specimen. The absorbance was then measured, and the specimens were returned to a water bath (37 °C) for the remaining time of the experiment. Further absorbance readings of the experimental groups were conducted at 10, 15, and 20 h after the initial incubation. Alginate-dye mix was used as a 100% control reference value for the release.

2.5. Antimicrobial Peptides

Antimicrobial peptides, LL-37 and SAAP-148, were purchased (Isca Biochemicals, Exeter, United Kingdom) in lyophilized form and were stored at −20 °C. Upon use, they were dissolved in Gibco 10× Dulbecco's phosphate-buffered saline (DPBS, Thermo Fisher Scientific, Landsmeer, The Netherlands), passed through 0.2 µm filter, and stored in aliquots at −80 °C. For cell culture, the peptides were further diluted in 10× DPBS and the respective cell culture media to the desired concentrations. The final concentration of 10× DPBS in the cell culture media was 1 vol% (including control conditions).

2.6. Reference In Vitro Cell Culture Conditions

For expansion purposes, murine macrophages J774A.1 (Sigma Aldrich, Zwijndrecht, The Netherlands) were precultured in the Dulbecco's Modified Eagle Media (DMEM, Thermo Fisher Scientific, Landsmeer, The Netherlands) supplemented with 1% penicillin/streptomycin (Pen/Strep, Thermo Fisher Scientific, Landsmeer, The Netherlands) and 10% fetal bovine serum (FBS, Thermo Fisher Scientific, Landsmeer, The Netherlands) at 37 °C, 5% CO_2, and normal oxygen levels for 5–7 days and were refreshed twice per week. Cell passages 12–14 were used for the experiments. At the end of preculture, the cells were detached using a cell scraper, counted, and were seeded for the follow-up experiments. Polarization of macrophages was performed through addition of 100 ng ml^{-1} of LPS and 10 ng ml^{-1} of IFN-γ into the DMEM to obtain M1 pro-inflammatory phenotype, and 10 ng ml^{-1} of IL-4 for the anti-inflammatory M2 phenotype. Unpolarized and untreated cells were referred to as M0.

Murine preosteoblast cells MC3T3-E1 (Sigma Aldrich, Zwijndrecht, The Netherlands) were precultured in α-Minimum Essential Media (αMEM, Thermo Fisher Scientific, Landsmeer, The Netherlands) without ascorbic acid and were supplemented with 1% Pen/Strep and 10% FBS at 37 °C and normal oxygen levels for 5–7 days and were refreshed twice per week. Cell passages 11–14 were used for the experiments. Following the preculture, the cells were harvested, counted, and seeded for the follow-up experiments. Non-osteogenic medium containing αMEM was used for the first two days of culture after which it was replaced by osteogenic media for the remaining duration of the cell culture experiments. The osteogenic media contained αMEM, 50 µg ml^{-1} of ascorbic acid (Sigma Aldrich, USA), and 4 mM of β-glycerophosphate (Sigma Aldrich, Zwijndrecht, The Netherlands). The flasks and well plates were all purchased from Greiner Bio-One (Alphen aan den Rijn, The Netherlands).

2.7. Cytocompatibility of Antimicrobial Peptides

The J774A.1 cells were seeded in a 48-well plate at a density of 5000 cells per well and were cultured for 5 days to reach partial confluency. On day 5, the cells were polarized toward the M1 phenotype. On day 6 various concentrations of LL-37 and SAAP-148 were introduced to the cells. Similarly, 5000 MC3T3-E1 cells per well were seeded in a 48-well plate. After 24 h, the peptides were added to the culture.

To confirm and compare the cytotoxicity levels of LL-37 and SAAP-148, both cell lines were exposed to 0.1, 1.0, 4.0, and 10.0 µM of each peptide for 7 days and were refreshed twice per week with fresh peptide-containing media. The assessments were carried out after 1, 3, and 7 days of culture with the peptides using the Presto Blue assay (Thermo Fisher Scientific, Landsmeer, The Netherlands) to measure metabolic activity and optical microscopy (ZOE Fluorescent Cell Imager, Bio-Rad Laboratories B.V., Veenendaal, The Netherlands). Additionally, a viability/cytotoxicity assay (Live/Dead, Thermo Fisher Scientific, Landsmeer, The Netherlands) was performed at the end of the experiment (after 7 days). The cells cultured in the reference media were used as controls to assess the viability of the cells cultured with the different concentrations of peptides. Two independent experiments, each time with replicates of four, were conducted to ensure the obtained results are reproducible.

The assessment was carried out according to the ISO 10993 standard intended for the biological evaluation of medical devices for in vitro cytotoxicity.[32] The standard quantitatively defines cytotoxicity as a condition with more than 30% reduction in cell viability (cellular metabolic activity, live/dead staining) and provides guidelines for qualitative morphological grading (optical microscopy, SEM).

2.7.1. Presto Blue Metabolic Assay

Briefly, the cultured cells were incubated with 10% of Presto blue solution in cell media for 1 h. The media was then transferred into a 96-well plate and the metabolic activity was read at an excitation wavelength of 535 nm and an emission wavelength of 590 nm using a VICTOR X3 Multilabel Plate Reader (PerkinElmer Nederland B.V., Groningen, The Netherlands). Blank value (medium without cells) was subtracted from the obtained values and the relative metabolic activity was calculated with reference to the control condition (100%).

Table 1. An overview of the assessed mouse genes and their primer sequences.

Gene	Primer sequence—forward	Primer sequence—reverse
Ubc (housekeeping gene)	*agcccagtgttaccaccaag*	*acccaagaacaagcacaagg*
Il-1β	*gcaccttacacctaccagagt*	*aaacttctgcctgacgagctt*
Il-6	*ctgcaagagacttccatccag*	*agtggtatagacaggtctgttgg*
Il-10	*ccaagccttatcggaaatga*	*ttttcacaggggagaaatcg*
Il-12	*aggtgcgttcctcgtagaga*	*aaagccaaccaagcagaaga*
Tgf-β	*ccacctgcaagaccatcgac*	*ctggcgagccttagtttggac*
Tnf-α	*ctgaacttcggggtgatcgg*	*ggcttgtcactcgaattttgaga*
Runx2	*cggtctccttccaggatggt*	*gcttccgtcagcgtcaaca*

2.7.2. SEM Imaging

The cultured cells were washed twice with 1× DPBS and were fixated with 4% formaldehyde solution (Sigma Aldrich, Zwijndrecht, The Netherlands). They were then washed with demineralized water and dehydrated with 50% ethanol (15 min), 70% ethanol (20 min) and 96% ethanol (20 min). The samples were left to dry overnight.

2.7.3. Live/Dead Staining

The cultured cells were washed with 10× DPBS and then with 1× DPBS. The viability/cytotoxicity solution containing 2 µM Calcein AM and 3 µM EthD-1 in 1× DPBS was added to each well. After 30 min of incubation at 37 °C, it was replaced by 1× DPBS and the cells were imaged on a on ZOE Fluorescent Cell Imager.

2.8. Effects of Antimicrobial Peptides on Macrophage Polarization

The unpolarized J774A.1 cells were cultured with each peptide at their minimal bactericidal concentration (MBC = 1.6 µM)[21,33] for 4 and 24 h, to assess and compare the immunomodulatory potency of both peptides at their bactericidal levels. The timepoints of 4 and 24 h were selected to simulate the exposure of the cells to the peptides following a burst release. The effects were evaluated through RT-qPCR by assaying the expression of pro-inflammatory (*Tnf-α, Il-6, Il-12, Il-1β*) and anti-inflammatory (*Tgf-β, Il-10*) mouse genes and were compared with phenotype-specific morphology by optical imaging on ZOE Fluorescent Cell Imager. An overview of the genes and the primer sequences is presented in **Table 1**.

The J774A.1 cells were seeded in 24-well plates at the density of 20 000 cells per well. After 3 days of culture in reference conditions, one group of unpolarized cells (M0 phenotype) was immediately stopped and served as an initial control condition (M0t0). The remaining cells were divided into experimental groups based on the peptide or polarization treatment, which were thereafter incubated for 4 or 24 h (t4, t24): untreated M0 (M0t4, M0t24), M1 polarized (M1t4, M1t24), M2 polarized (M2t4, M2t24), and M0 cells treated with LL-37 (LLt4, LLt24) or SAAP-148 (SAAPt4, SAAPt24).

Unpolarized (M0), M1, and M2 polarized cells served as controls for the conditions where cells were cultured with either of the peptides. Two independent experiments were performed with replicates of three.

2.8.1. Gene Expression Analysis: RNA Isolation, cDNA Synthesis, and RT-qPCR

At every time point, RNA isolation was performed. The cultured cells were homogenized with TRIzol and were scraped. The isolation was performed according to a customized protocol combined with washing steps from RNeasy kit (QIAGEN Benelux B.V, Venlo, The Netherlands). The amount of eluted RNA was measured using a UV/vis spectrophotometer (QIAxpert, QIAGEN Benelux B.V, Venlo, The Netherlands).

QuantiTect Reverse Transcription kit (QIAGEN Benelux B.V, Venlo, The Netherlands) was used for cDNA synthesis. The obtained cDNA was then mixed with primers (Table 1) and 2× QuantiNova SYBR green PCR master mix (QIAGEN Benelux B.V, Venlo, The Netherlands) according to the manufacturer's instructions and was amplified with 42 temperature cycles at 95 °C and 60 °C. The relative gene expression was then calculated from the obtained cycle threshold (Ct) values using the Delta-Delta Method.

2.9. Effects of Antimicrobial Peptides on Bone Regeneration

The MC3T3-E1 cells (10 000 cells per well) were seeded in a 24-well plate and were cultured for two days. Then, they were divided into four experimental groups cultured for another 8 days (10 days in total), and refreshed twice per week (with fresh peptides, if applicable per condition). The first group was intended for observation of any possible effects of the peptides (1.6 µM) on early osteogenic differentiation. Therefore, the cells were incubated with the peptides for 24 h on day 2 (LL-D2-24 h, SAAP-D2-24 h) after which they were switched to osteogenic media without the peptide. To compare it with the later role of the peptides in osteogenic differentiation, the second group (LL-D9-24 h, SAAP-D9-24 h) was cultured in osteogenic media until day 9 and was incubated with the peptides only for the last 24 h of the experiment. The last group (LL-D2-D10, SAAP-D2-D10) was treated with the peptides from day 2 till day 10 to check for any impacts due to sustained exposure. On day 10, the cells were analyzed for the expression of *Runx2* gene (using the same protocol as described in Section 2.8.1) and were stained to analyze the secretion of the same protein.

As controls for the cells exposed to the peptides, a group of cells was cultured for the whole duration of the experiment in osteogenic media without any peptide. Two independent experiments were performed with replicates of three.

2.9.1. RUNX2 Immunocytochemical Staining

After completing cell culture, cells were washed with 1× DPBS and were fixated with 4% formaldehyde solution (Sigma Aldrich, Zwijndrecht, The Netherlands). The further preparation for fluorescent staining was as follows: the cells were permeabilized with

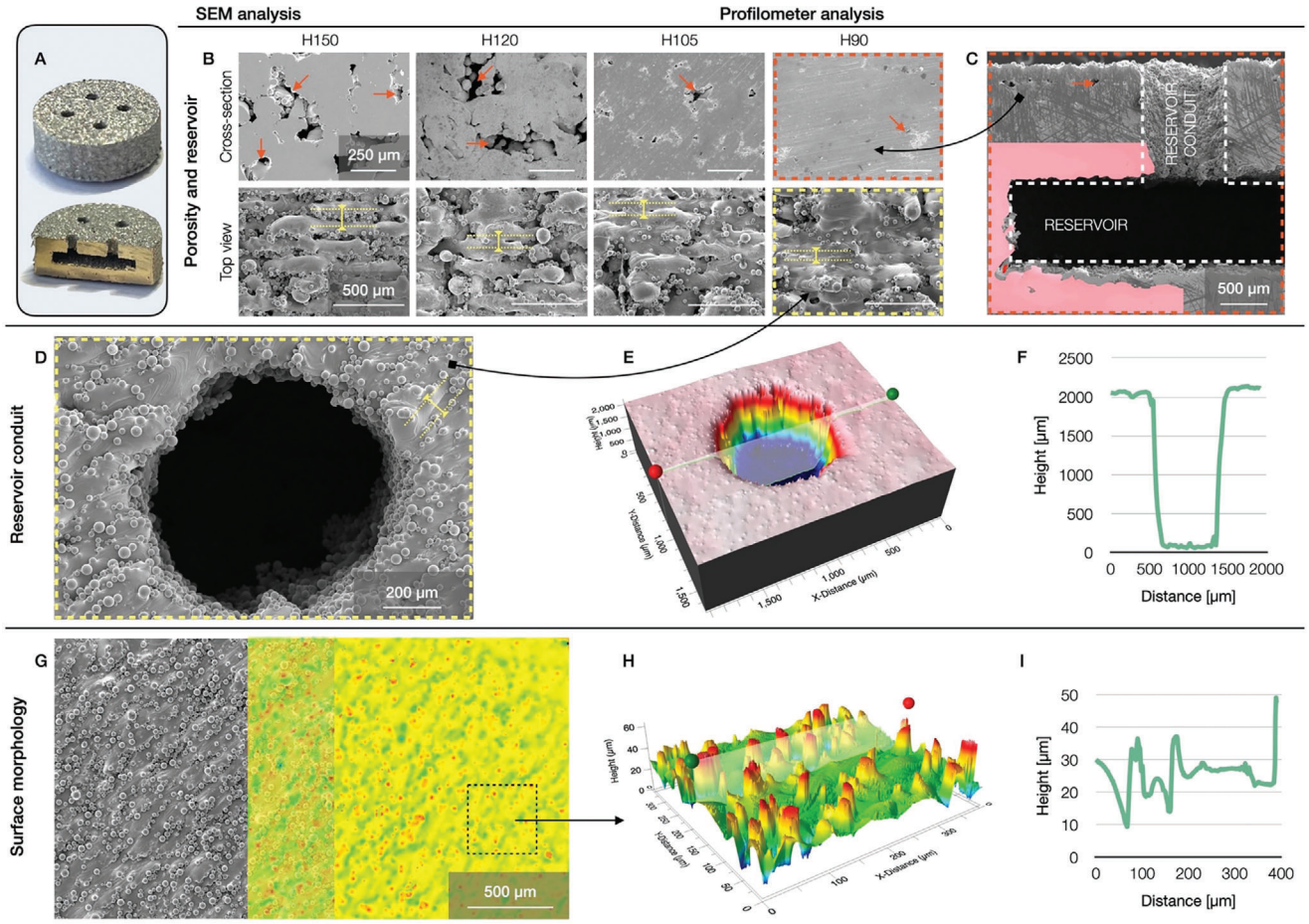

Figure 2. Characterization of the 3D printed samples by SEM and optical profilometer: A) An image of the 3D printed sample and its cross-section; B) The sequence of images indicating the porosity (red arrows) as the hatching distance (yellow lines) decreased from 150 to 90 µm); C) Cross-sectional area of a sample printed with the final printing parameters depicting the reservoir and the conduit; The reservoir and its conduit were similarly imaged using D) SEM and E) profilometer, including F) a depth line profile of the reservoir with a conduit; G) An overlay image of SEM/profilometer showing the printing direction and typical surface roughness; H) A 3D reconstruction of the surface and I) an example of line profile of the surface roughness, both from the optical profilometer.

0.5% Triton/PBS (Sigma Aldrich, Zwijndrecht, The Netherlands) for 5 min at 4 °C and 1% BSA/PBS (Sigma Aldrich, Zwijndrecht, The Netherlands) was added as a blocking buffer for 5 min at 37 °C. The rabbit recombinant monoclonal RUNX2 primary antibody (Abcam B.V., Amsterdam, The Netherlands) was diluted to 1:250 in 1% BSA/PBS and was incubated with the cells for 1 h at 37 °C. The cells were then washed 3 times with 0.5% Tween/PBS (Sigma Aldrich, Zwijndrecht, The Netherlands) and were incubated with the Alexa Fluor 488 Donkey anti-Rabbit secondary antibody (Thermo Fisher Scientific, Landsmeer, The Netherlands) diluted in 1:200 in 1% BSA/PBS for another 1 h at room temperature in the dark. Finally, the cells were washed three times with 0.5% Tween/PBS and were imaged on ZOE Fluorescent Cell Imager (Bio-Rad Laboratories B.V., Veenendaal, The Netherlands).

2.10. Statistical Analysis

The obtained data was plotted using GraphPad Prism 8.0 (GraphPad Software, USA). The plots represent mean value ± standard deviation. The statistical significance of the data was evaluated using one-way and two-way ANOVA tests, with Bonferroni correction. The results were considered statistically significant when $p < 0.05$.

3. Results

3.1. Morphological Characterization

The fabricated implant specimens including the reservoir are depicted in **Figure** 2A. The porosity of the 3D printed samples was qualitatively assessed by observing the changes in the surface morphology and the pore size in the sample cross-section (Figure 2B and C). The greatest reduction of pores was observed with a hatching distance of 90 µm. As the hatching distance increased (105, 120, and 150 µm), shown in the figure for comparison, the samples demonstrated greater distance between the printing lines (indicated in the top row of images with yellow lines) and more frequent presence of large pores (bottom row of images with red arrows indicating the pores). Based on these

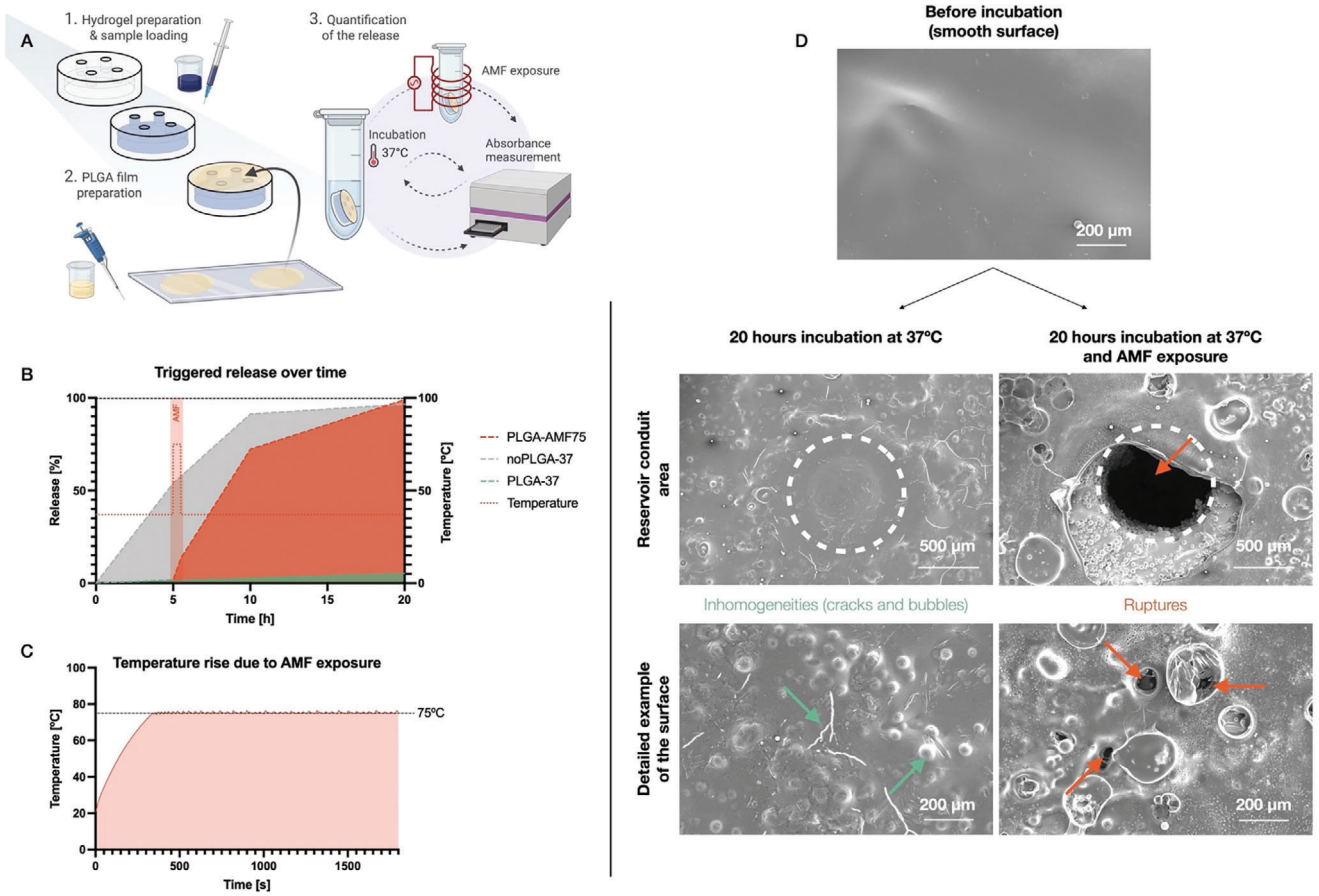

Figure 3. The workflow and results of the on-demand release experiment: A) A schematics drawing illustrating the preparation of the hydrogel-dye loaded samples with a PLGA film and the subsequent release measurements; B) Data on the release kinetics differences between the experimental groups; C) A plot of the data illustrating the rise of temperature due to exposure to an alternating magnetic field; and D) SEM images comparing the surfaces before incubation, after 20 h of incubation, and after 20 h of incubation with AMF exposure. Created with BioRender.com.

results, a hatching distance of 90 µm was selected and further characterized.

The diameter and depth of the reservoir conduits were measured to be 905 ± 26 µm and 1028 ± 35 µm, respectively (Figure 2D,E). The height of the reservoir was determined to be 996 ± 54 µm. The total height of the reservoir with the conduit is depicted in the cross-section overlay image (Figure 2C) and in the vertical line profile of the cross-section (Figure 2F).

The surface morphology, as well as the geometry of the inner features, were assessed by SEM and optical profilometry (Figure 2G–I). The visualization of the surface by SEM showed a morphology typical for the SLM fabrication method, with partially molten residual metal powder. The same was observed in the surface analysis performed by the optical profilometer, as depicted in the overlay image with SEM (Figure 2G). The 3D reconstruction of the surface by the profilometer and an example of the surface vertical cross-section profile (Figure 2H,I) illustrate the heterogeneity of the surface. For the quantitative analysis of the surface roughness (summarized in **Table 2**), the arithmetic mean height (S_a) was determined to be 5.0 ± 0.5 µm, with a maximum peak-to-valley height (S_t) of 62.5 ± 4.7 µm. The peak height (S_p = 35.0 ± 4.5 µm) was higher than the valley depth (S_v = 27.0 ± 6.8 µm), corresponding with the partially molten residual powder.

Table 2. The results of the surface roughness measurement performed using an optical profilometer. The data represent the mean ± SD.

Parameter	Symbol	Value [µm]
Peak height	S_p	35.0 ± 4.5
Valley depth	S_v	27.0 ± 6.8
Maximum peak to valley height	S_t	62.5 ± 4.7
Arithmetic mean height	S_a	5.0 ± 0.5

3.2. Kinetics of On-Demand Drug Release

The absorbance measurements demonstrated the differences in the release kinetics throughout the monitored period among the three experimental groups (Figure 3B). Samples with no PLGA film (noPLGA-37) incubated at 37 °C enabled a burst release throughout the first 5 h releasing over 50% of the model molecule. By the end of the monitoring period (i.e., after 20 h),

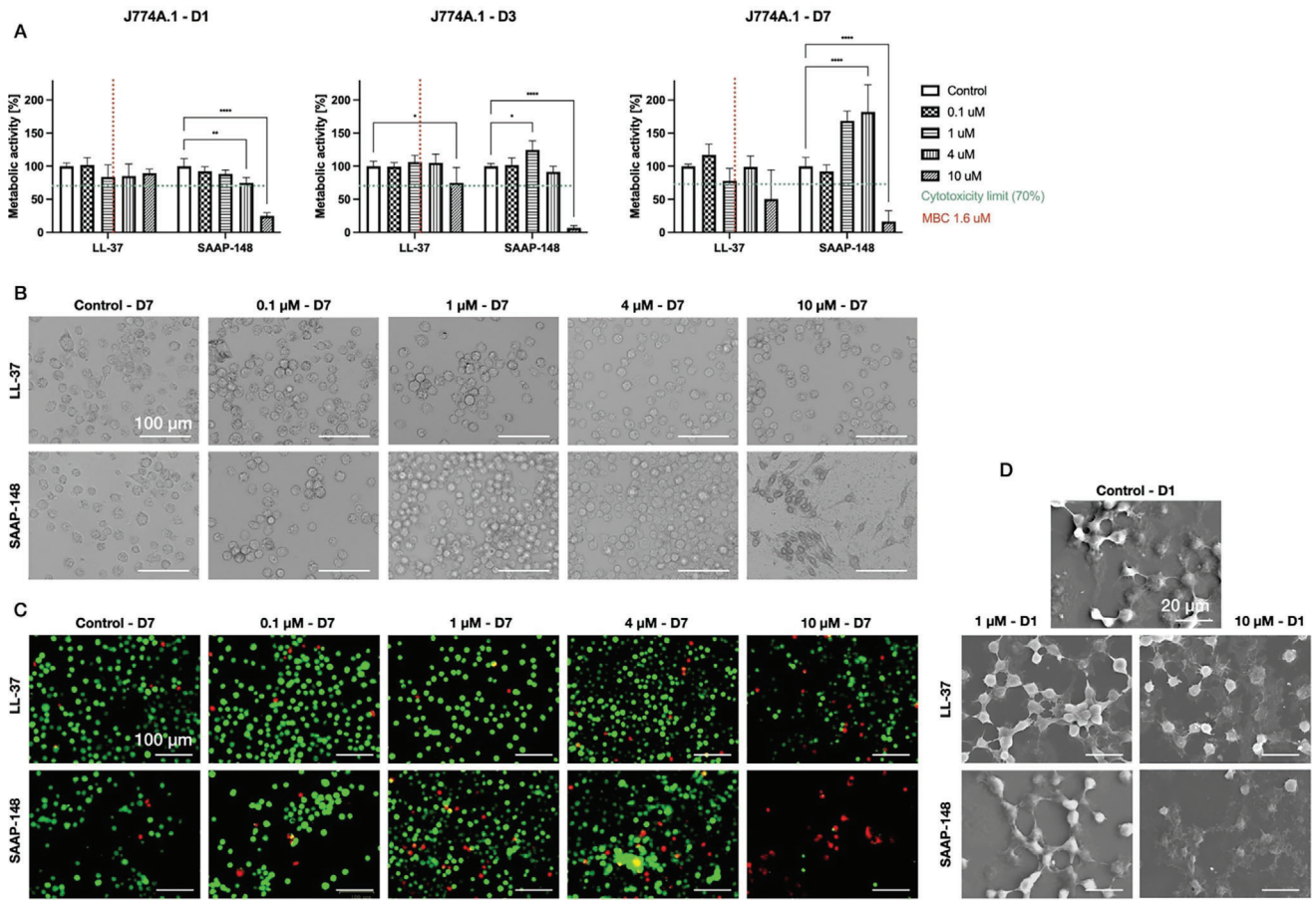

Figure 4. Data on the cytotoxicity of LL-37 and SAAP-148 toward J774A.1 cells. A) The relationship between metabolic activity and peptide concentrations measured after 1, 3, and 7 days of cell culture with the peptides; the data represent the mean ± SD; B) Optical images and C) live/dead staining after 7 days of culture with the peptides; D) The SEM images of the cells after 24 h of culture with 1 or 10 µM of LL-37/SAAP-148. Optical images for the 1- and 3-day timepoints are presented in Figure S1A,B (Supporting Information).

they released 97% of the available drug, in contrary to the specimens covered by a PLGA film which released only 5% of the model molecule. Exposure of the PLGA film-covered samples to the AMF (PLGA-AMF75) led to a rapid release of the model molecule in the next 4 h due to the collapse of the PLGA film by heating, releasing 99% of the model molecule by the end of the experiment.

The temperature transient curve measured in the solution, generated by the eddy currents in the Ti6Al4V implant in the presence of the AMF, is depicted in Figure 3C. After an initial temperature rise, with an average rate of 9.6 °C min^{-1}, the temperature stabilized at 75.0 ± 0.4 °C for the remaining period of the 30-min exposure.

The SEM images support the above-described results (Figure 3D). Before the incubation, the film appeared to be smooth and without any visible pores/cracks. After 20 h of incubation at 37 °C, the film has developed some inhomogeneities (very small pores and bubbles in the film), however, no large holes were observed. In contrast to that, PLGA film subjected to the heating generated by the AMF-induced eddy currents in the Ti6Al4V sample, underwent irreversible changes with some holes having the same size as the reservoir conduits, likely due to the shrinkage of the film.

3.3. Cytotoxicity of the Antimicrobial Peptides

3.3.1. Cytotoxicity of Peptide toward Macrophages

The results of the Presto Blue assay (**Figure** 4A) showed that the metabolic activity of the macrophages was maintained above a threshold of 70% throughout the first three days of culture even with the highest concentration of LL-37 tested (i.e., 10 µM) but dropped to about 50% on day 7. On the contrary, the cells suffered a significant reduction in metabolic activity (i.e., 75%) after an analogous exposure to 10 µM of SAAP-148, already after one day of culture. The damage caused by the synthetic peptide was visible in the optical microscopy images (Figure 4B) as cells appeared darker and seemed to have lost their typical morphological features. SEM images comparing the cells exposed to 1.0 and 10.0 µM of both AMPs confirmed the loss of the round shape typical for macrophages (Figure 4D). Similarly, the live/dead staining images (Figure 4C) indicated a strong decline in the total number of viable cells for 10.0 µM of SAAP-148. Together with the qualitative morphological grading (summarized in **Table** 3), the results suggest that the in vitro cytotoxicity thresholds of both LL-37 and SAAP-148 against macrophages lay between 4.0 and 10.0 µM while prolonged exposure to lower concentrations of SAAP-148

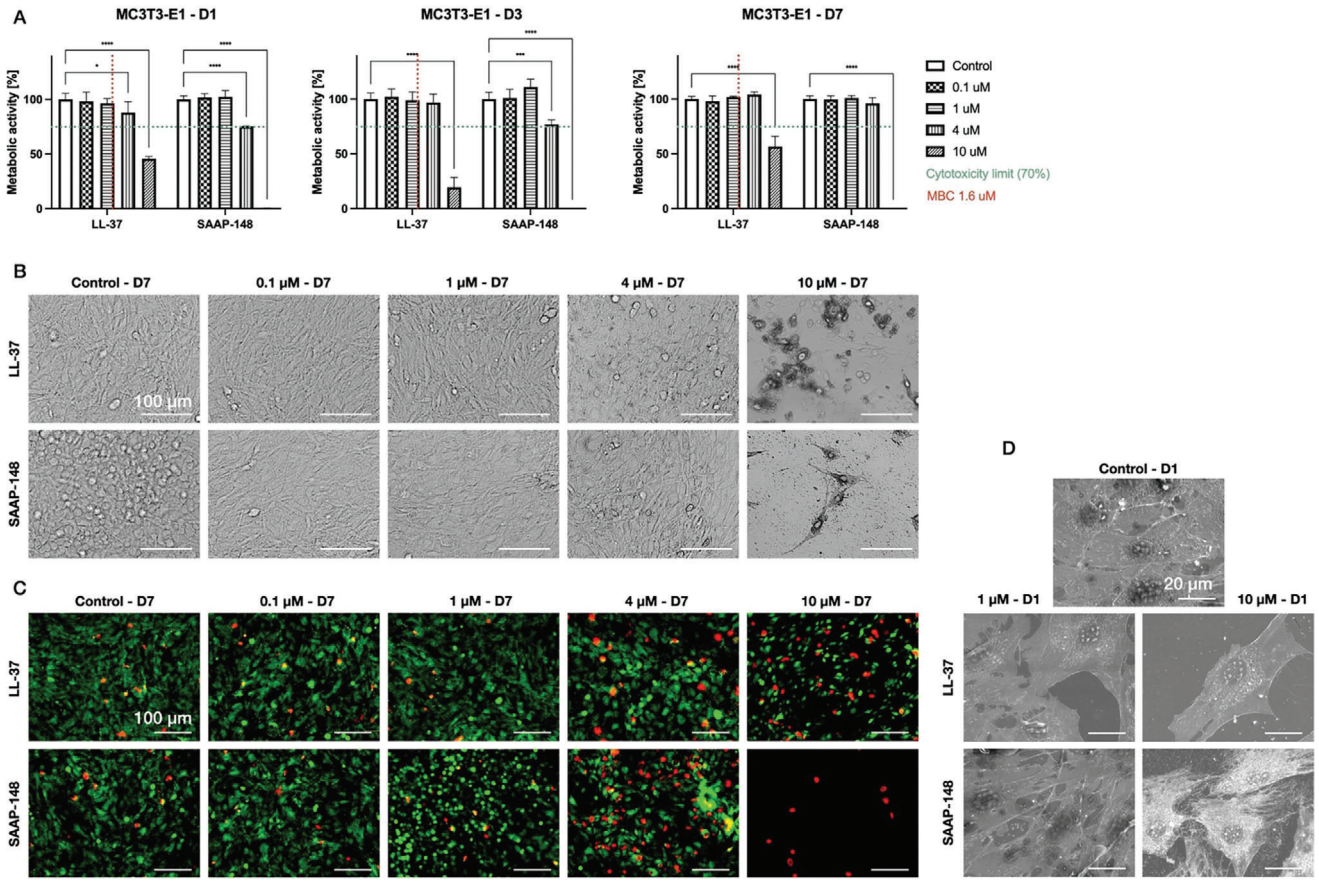

Figure 5. Data on the cytotoxicity of LL-37 and SAAP-148 toward the MC3T3-E1 cells. A) Relationship between metabolic activity and peptide concentrations measured after 1, 3, and 7 days of cells culture with the peptides; the data represent the mean ± SD; B) Optical images and C) live/dead staining after 7 days of culture with peptides; D) The SEM images of the cells after 24 h of culture with 1 or 10 µM of LL-37/SAAP-148. Optical images for the 1- and 3-day timepoints are in presented Figure S1C,D (Supporting Information).

Table 3. Qualitative assessment of the cytotoxicity of the peptides.

Cell type	Peptide concentration [µM]	LL-37	SAAP-148
Macrophages	0.1	None	None
Preosteoblasts		None	None
Macrophages	1.0	None	None
Preosteoblasts		None	None
Macrophages	4.0	None	None
Preosteoblasts		Slight	Mild
Macrophages	10.0	Mild	Severe
Preosteoblasts		Moderate	Severe

(i.e., 1–4 µM for 3 to 7 days) boost the metabolic activity of those cells with regard to control.

3.3.2. Cytotoxicity of Peptides toward Preosteoblasts

Preosteoblasts showed a higher degree of sensitivity to the peptides as compared to the macrophages (**Figure 5** and Table 3). The metabolic activity of preosteoblasts stayed below 70% with 10.0 µM of both peptides throughout the whole culturing period and even the 4.0 µM of SAAP-148 placed the cells at the cytotoxicity border on day 1 and day 3 (Figure 5A). Just like for macrophages, optical imaging confirmed the adverse effects of the high concentration (10.0 µM) of both peptides on the cellular morphology of preosteoblasts (Figure 5B) as well as lower cell numbers. In SEM, the cells exposed to 10.0 µM of SAAP-148 appeared white instead of translucent/grey color (Figure 5D). As the concentration of the peptides increased, the number of dead cells grew, and no live cells were detected with 10.0 µM of SAAP-148 (Figure 5C). The higher sensitivity of preosteoblasts defined the cytotoxicity threshold to be around 4 µM for SAAP-148 and in the range of 4–10 µM for LL-37.

3.4. Effects of Antimicrobial Peptides on Macrophage Polarization

The M0 cells showed almost no expression of the selected pro-inflammatory markers *Il-1β*, *Il-6*, *Il-12* or *Tnf-α* after 4 and 24 h of culture with either of the peptides (**Figure 6**A). The expression of the anti-inflammatory markers *Il-10* and *Tgf-β* was not different between both peptides, and the levels of expression were around

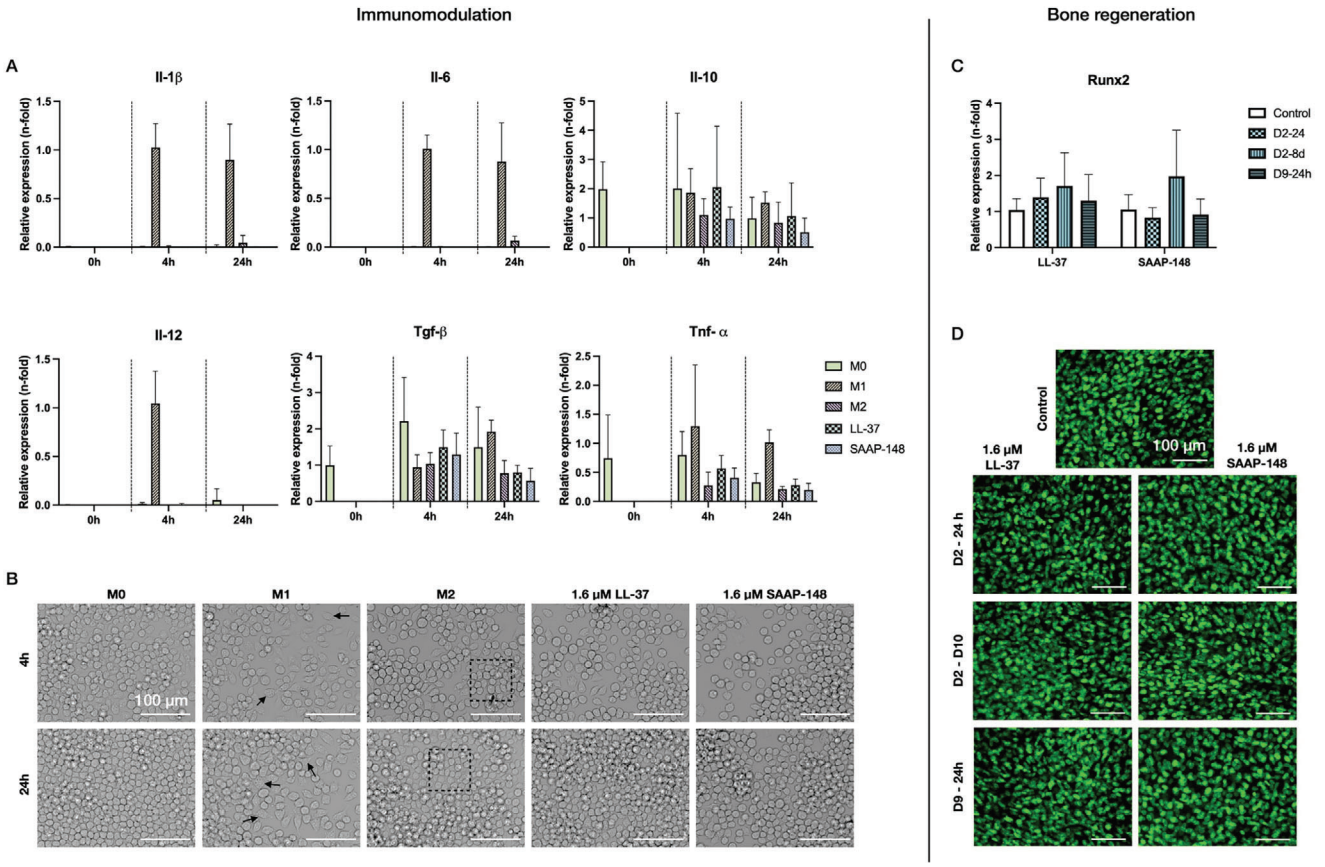

Figure 6. Data on the osteoimmunomodulatory activity of LL-37 and SAAP-148. A) The expression of M1- and M2-specific genes by the J774A.1 cells in various experimental conditions; B) The optical images of the macrophages under various experimental conditions; C) *Runx2* expression in MC3T3-E1 and D) the immunocytochemical staining of RUNX2 in MC3T3-E1. The gene expression data represent the mean ± SD.

the same values as for the cells polarized toward M2 (*Il-4*). The optical images of cell morphology showed no changes in shape with regards to M0 cells (Figure 6B). The overall results of the cell profile suggest that neither peptide is capable of eliciting strong proinflammatory response, and there is rather a trend in directing the cells toward their anti-inflammatory phenotype, although not significant.

3.5. Effects of Antimicrobial Peptides on Preosteoblasts Differentiation

The expression of *Runx2*, a known early osteogenic marker, did not reveal any significant differences among the different exposure conditions, although longer incubation with both peptides showed a statistically insignificant trend in promoting the differentiation of osteoblastic cells (Figure 6C). The results were in line with the immunocytochemical staining (Figure 6D).

4. Discussion

The relatively low rates of IAI occurrence as we know them today are expected to rapidly transform in the future alongside the increasing incidence of resistant organisms, not only in IAI but in all acquired infections.[13] To navigate through the path of averting it, researchers have been striving to identify alternatives that would allow for a reduction in the use of antibiotics or for their replacement altogether with substitutes with lesser propensity to resistance development.[18] The incredible adaptability of pathogenic microorganisms has, however, been able to catch up with many initially promising discoveries. Today, it is known that bacteria may be able to become resistant to silver particles,[34,35] which have and are still believed to be a very potent antibacterial agents, and acquire tolerance to some widely used alcohol-based hospital handwashes.[36] Therefore, new approaches and mechanisms for delivering antimicrobial agents, which will minimize the likelihood of further AMR spread, are stringently needed.

4.1. On-Demand Drug Delivery

The concept proposed in this study promises to overcome some of the above-mentioned limitations by enabling local drug release when needed, i.e., only in cases when infection is detected, thereby limiting unnecessary exposure. Through the incorporation of surface reservoirs into the 3D printed Ti6Al4V samples, the drug is protected from external adverse factors which may inactivate or degrade it completely or scrape it from the surface (as in the case of surface coatings) during the rough process

of surgical implantation. Furthermore, the large proximal area would be at the disposal of bone cells, allowing establishment of a proper connection between the newly formed tissue and the biomaterial. It also leaves room for further biofunctionalization of the surface to promote bone regeneration, such as incorporating osteogenic elements,[37–39] or further enhancing the antibacterial capacity of the surface indirectly by equipping the surface with immunomodulatory cues.[40] Moreover, on-demand release of antibacterial agents can ensure the delivery of a therapeutic dose upon infection detection instead of a continuous release of antibiotics and consequently greater exposure to subtherapeutic doses in the cases when the infection does not occur immediately.

The proof-of-concept experiment performed here demonstrated the workability of such system. The reservoir incorporated into the Ti6Al4V specimens could be loaded with a substance, such as hydrogel containing a drug, and covered with a protective film to prevent release. As a mode of activation for the drug release, heat generated through an AMF was selected. AMF fulfills the set functional requirements as a suitable trigger for the drug release from an implant inserted in the bone tissue. It demonstrates localized heating contained to the implant and its immediate proximity, and penetrates through the involved tissues (including bone tissue) without damaging it or causing discomfort, as long as the applied parameters are within the defined biological safety limits.[41,42] In comparison to other modes of activation that are used for surface triggering (such as light),[43] magnetic fields can more effectively penetrate through the involved tissues and reach the implant without energy attenuation,[44] which may otherwise limit the efficiency of the release. Furthermore, the produced heat may also target and aid the elimination of the bacteria adhered to the implant's surface.[45] With regard to the effect of the AMF on mammalian cells, a study by Sanz *et al.* has reported no changes in the morphology of neuroblastoma cells after 30 min of exposure to an AMF with frequency of 570 kHz and field strength of 23.9 kAm^{-1}.[46] To cover the loaded reservoirs, PLGA was chosen as it fulfills our functional requirements. First, its glass transition temperature (T_g) is in the range of 50–80°C[47,48] and it is a biocompatible biomaterial frequently utilized in many biomedical applications.[49] Furthermore, due to its hydrophobic character, the hydrolysis-driven degradation is restricted to its surface rather than to the bulk, thereby reducing the drug release.[50,51] As a result of those requirements, we concluded that PLGA was a suitable biomaterial for this proof-of-concept study.

Upon untethered activation of the delivery system through an AMF, the protective film collapsed, allowing the drug to be released from the reservoir. In this system, eddy currents in the titanium implant were utilized to generate a sufficient level of temperature increase. Temperature rise instigating the glass transition of the PLGA is believed to have driven the release of the model molecule,[49] considering the thermodynamic properties of PLGA ($T_{g(PLGA50:50)}$ = 46–50 °C, according to the manufacturer; degradation temperature $T_{d(PLGA50:50)}$ >200 °C according to the literature)[52] and the images showing the shrinkage of the film, an effect associated with the glass transition process.[48] In this study, some release was also detected for the capped samples, which can be due to slow gradual shrinkage of the PLGA and could be further improved by increasing the T_g, increasing the thickness of the PLGA film, and modifying other geometrical design parameters.

All in all, such an on-demand release system could be combined with AMPs and integrated into orthopedic implants to treat infections that may onset several days to several weeks after the surgery, by delivering a high dose of AMPs for a short period of time into the surroundings, instead of a systemic administration of antibiotics or continuous local release from an exposed local drug delivery system.

4.2. Additive Manufacturing and Characterization of Surface Reservoirs

The assessment of the fabricated samples in this study showed deviations of up to 121 μm (6%–12%) from the designed dimensions, which represents a medium dimensional accuracy based on the ISO 2768,[53] and are somewhat better than the deviations reported in the literature (150–195 μm).[54,55]

The laser powder bed fusion additive manufacturing processes including the one used here (i.e., SLM or direct metal printing) endow products with a certain degree of roughness. The characteristic surface roughness observed in this study (S_a = 5.0 ± 0.5 μm) is within the range of values reported in the literature (5–9 μm)[56–59] and is likely to facilitate the attachment of osteoblastic cells, which prefer rough topographies mimicking the bone environment.[60,61] Porosity, correlating with surface roughness, was successfully minimized by decreasing the hatching distance of the laser beam,[55] to prevent any leakage of the drug from the reservoirs. Further reduction of roughness and porosity could be achieved by decreasing the powder bed thickness, decreasing the powder size, and employing greater laser power.[59,62,63]

4.3. LL-37 and SAAP-148 as Potential Drug Candidates

To maximize the strengths of the proposed concept aiming to decrease the spread of AMR, the antibacterial agent of choice, intended to be placed into the reservoirs, must be superior to antibiotics in its predisposition to resistance development. Some AMPs have demonstrated the ability to withstand repeatable exposures to bacteria without eliciting resistance in them.[21] The failed struggle of bacteria to adapt to AMPs is attributed to the larger molecular size and more complex and simultaneous modes of action employed by such molecules against the bacteria, in comparison to conventional antibiotics.[64] Despite this tremendous quality, not many AMPs have managed to enter the market as a consequence of the current regulatory standard, which devalue the AMPs due to their relatively lower efficacy (with respect to antibiotics).[18,64] Nevertheless, this is likely to change in the future as AMPs are increasingly capturing the interest of researchers, potentially yielding new formulations.

LL-37 is one of the naturally occurring AMPs, whose properties have been extensively investigated in vitro and some of its formulations were eventually tested also in clinical trials.[65] Therefore, it was chosen for a comparative assessment of its properties with SAAP-148. Owing to its cationic character, LL-37 can interact with mammalian cell membranes, bestowing it with

concentration- and cell type-dependent cytotoxicity. According to the published data, the cytotoxicity levels of this peptide against immune cells are in the range of 13–40 μM,[29,66,67] which are higher than the results of this study obtained with murine macrophages which suggest (4–10 μM). The discrepancies may be attributed to the cell type utilized in the experimental setups, possibly leading to distinct cell response and peptide tolerance,[67] or shorter exposure of cells to the peptides (only up to 24 h).[66,67] To draw a direct comparison with the experiments presented in this study, even the highest concentration of LL-37 (10.0 μM) did not demonstrate any cytotoxic effects on macrophages after 24 h. Monitoring cells for up to 7 days, however, showed variable cell tolerance of peptides over time.

Assessment of the cytotoxicity of LL-37 against murine preosteoblasts showed higher sensitivity of these cells at 10 μM and the results are close to the data available in the literature, which reports cytotoxicity thresholds of around 2.7–4 μM against osteoblast cells.[68–70]

Angiogenic, wound healing, and immunomodulatory activity are some of the other attributes ascribed to many AMPs, alongside their antibacterial activity. LL-37 has shown to possess immunomodulatory effects, such as enhancing M1 polarization[71] and recruitment[29,33,72] of immune cells, with other studies addressing the role of the peptide in osteogenic differentiation.[73–76] On the contrary, the LL-37-stimulated cells assessed in this study resembled more and carried expression markers profile similar to M2 control cells, which is in line with a study from Mookherjee *et al.* who observed suppression of proinflammatory cytokines, such as *Tnf-α*, *Il-6* and *Il-1β* by LL-37.[77] Furthermore, osteogenesis-related gene expression analysis showed only insignificant trend.

Cytotoxicity is one of the drawbacks of the natural peptides alongside their in vivo susceptibility to protease-mediated degradation and impaired antibacterial activity in plasma.[21,28] To overcome such weaknesses, synthetic antibacterial peptides have been designed to toughen the AMPs in terms of their resilience to environmental factors and strengthen their antibacterial efficacy in human plasma. SAAP-148 is one of the synthetic derivates of LL-37 and was first introduced in the literature in 2017.[20] To our knowledge, no studies reporting the cytotoxic effects of SAAP-148 against macrophage or osteoblast-like cells have been published. The cytocompatibility of SAAP-148 has, however, been tested using other cell types showing varying cytotoxicity thresholds ranging between an upper 4 μM (fibroblasts)[78] and down to as low as 0.23 nmol (fibroblasts and keratinocytes).[79] Additional indirect comparison can be performed with another synthetic AMP, KR-12, derived from the human cathelicidin LL-37, which are shown to be much less cytotoxic than SAAP-148, with tolerable concentrations of up to 223 μM[80] (in contrast to 4–10 μM of SAAP-148 determined in this study).

There is no published literature on the (osteo)immunomodulatory properties of SAAP-148, although other synthetic AMPs are reported to possess osteogenic properties.[80] In this study, macrophages cultured with 1–4 μM of SAAP-148 exhibited increased metabolic activity, indicating a potential augmenting role of this peptide in immunomodulatory processes. However, further gene expression analysis did not show any significant effects. Assessment of the early osteogenic differentiation of preosteoblasts indicated only an increasing trend of an osteogenic marker for SAAP-148 observed only over a long period of culturing and without a statistical significance.

To mitigate the adverse effects of natural AMPs against mammalian cells and at the same time boost their antibacterial potential, synthetic peptides are usually designed to possess higher binding specificity to bacterial cells.[33,81] In the assessment of both peptides included in this study, SAAP-148 showed stronger cytotoxicity at high concentrations against both cell types than its natural analogue LL-37 and sharply reduced the number of viable cells at concentrations > 4.0 μM. The cytotoxicity of these peptides is usually attributed to the hydrophobic interaction between the cell membrane and the peptide's hydrophobic amino acids and its cationic character.[33,66] Incorporating a higher number of hydrophobic and cationic sequences into the molecules is, however, the major mechanism used in the design of synthetic peptides to promote their antibacterial activity.[81] The sequences of both peptides are presented in Table S2 (Supporting Information). While LL-37 is comprised of nearly 30% and 13.5% of positively and negatively charged amino acids (AA), respectively, SAAP-148 carries 45% and 0% of positively and negatively charged AA, respectively. Therefore, the likelihood that SAAP-148 would be attracted to any slightly negative membrane, including mammalian cell membrane, is quite large.

All in all, both peptides demonstrated that their incorporation in orthopedic implants should lead to no adverse consequences on the bone regeneration process when used below the cytotoxic concentrations. Despite its slightly higher cytotoxicity, SAAP-148 represents a more suitable candidate for the application, as it has demonstrated higher antibacterial efficacy by maintaining its activity also in human plasma, unlike LL-37.[21] Moreover, the on-demand drug delivery system presented here should enable short drug exposures, thereby alleviating the adverse effects to host cells, even if the released concentrations would be close to the cytotoxicity limit. To precisely define the acceptable concentrations and exposure times for in vivo, the proposed on-demand delivery system must be further verified in an in vitro model resembling the physiological flow conditions, thereby considering the diffusion of the drug into the environment. in vivo experiments will, however, be needed to pave the way for clinical adoption of the proposed on-demand delivery system and the antimicrobial peptides.

5. Conclusion

This study introduced a novel concept for local on-demand drug delivery as a strategy to mitigate the risks presented by AMR and to ensure a therapeutic concentration is achieved. The designed samples were successfully fabricated using additive manufacturing, were loaded with a hydrogel and a model molecule, and were capped with a PLGA film to prevent undesired release. Upon subjecting the specimen to the eddy currents created by an AMF, rapid drug release was triggered. Such a system could be implemented to treat the onset of implant-associated infections several days or week after the surgery without a need for systemic administration of antibiotics or an invasive form of treatment. The experimental findings of the cytotoxicity of LL-37 and SAAP-148 peptides showed mild adverse effects with increasing concentration of both peptides against macrophages and preosteoblasts. SAAP-148 showed to be more cytotoxic than LL-37, nonetheless

still safe for use around its MBC levels. No significant effects on gene expression of macrophages (i.e., stimulation either to pro- or anti-inflammatory phenotype) and preosteoblasts (i.e., gene expression of an early osteogenic marker) were observed. Considering its bactericidal potential reported in the literature and its mild boosting effects on macrophages, SAAP-148 seems to be a better candidate for incorporation into the reservoirs for further studies.

Supporting Information

Supporting Information is available from the Wiley Online Library or from the author.

Acknowledgements

The authors would like to thank Ing. Kees Kwakernaak from the Materials Science and Engineering department at TU Delft for help with sample preparation. This publication is part of the project DARTBAC (with project number NWA.1292.19.354 of the research program NWA-ORC) which is (partly) financed by the Dutch Research Council (NWO).

Conflict of Interest

The authors declare no conflict of interest.

Data Availability Statement

The data that support the findings of this study are available from the corresponding author upon reasonable request.

Keywords

3D printing, antibiotic-resistance infections, antimicrobial peptides, drug delivery, implant-associated infections, orthopedic implants

Received: September 25, 2023
Revised: January 16, 2024
Published online: February 25, 2024

[1] C. R. Arciola, D. Campoccia, L. Montanaro, *Nat. Rev. Microbiol.* **2018**, *16*, 397.
[2] M. Franceschini, L. Pedretti, V. Cerbone, N. A. Sandiford, *Ann. Jt.* **2022**, *7*, 4.
[3] W. Zimmerli, P. Sendi, *J. Pathol. Microbiol. Immunol.* **2017**, *125*, 353.
[4] N. A. Sandiford, A. McHale, M. Citak, D. Kendoff, *Hip. Int.* **2021**, *31*, 286.
[5] S. M. Jafari, C. Coyle, S. M. J. Mortazavi, P. F. Sharkey, J. Parvizi, *Clin. Orthop. Relat. Res.* **2010**, *468*, 2046.
[6] A. M. Malhas, R. Lawton, M. Reidy, D. Nathwani, B. A. Clift, *Surgeon* **2015**, *13*, 250.
[7] T. Karachalios, G. Komnos, A. Koutalos, *EFORT Open Rev.* **2018**, *3*, 232.
[8] P. F. Dobson, M. R. Reed, *EFORT Open Rev.* **2020**, *5*, 604.
[9] M. Haque, M. Sartelli, J. Mckimm, M. Abu Bakar, *Infect. Drug Resist.* **2018**, *11*, 2321.
[10] S. Zhang, X. Qu, H. Tang, Y. Wang, H. Yang, W. Yuan, B. Yue, *Adv. Sci.* **2021**, *8*, 1.
[11] B. Li, T. J. Webster, *J Orthop Res* **2018**, *36*, 22.
[12] S. H. Podolsky, *Palgrave Commun.* **2018**, *4*, 124.
[13] C. J. L. Murray, K. S. Ikuta, F. Sharara, L. Swetschinski, G. Robles Aguilar, A. Gray, C. Han, C. Bisignano, P. Rao, E. Wool, S. C. Johnson, A. J. Browne, M. G. Chipeta, F. Fell, S. Hackett, G. Haines-Woodhouse, B. H. Kashef Hamadani, E. A. P. Kumaran, B. McManigal, S. Achalapong, R. Agarwal, S. Akech, S. Albertson, J. Amuasi, J. Andrews, A. Aravkin, E. Ashley, F. X. Babin, F. Bailey, S. Baker, et al., *Lancet* **2022**, *629*, 6736.
[14] M. Gatti, S. Barnini, F. Guarracino, E. M. Parisio, M. Spinicci, S. D'Arienzo, S. Forni, A. Galano, F. Gemmi, *Antibiotics* **2022**, *11*, 1.
[15] M. Cloutier, D. Mantovani, F. Rosei, *Trends Biotechnol.* **2015**, *33*, 637.
[16] S. W. M. A. I. Senevirathne, J. Hasan, A. Mathew, M. Woodruff, P. K. D. V. Yarlagadda, *RSC Adv.* **2021**, *11*, 1883.
[17] D. Campoccia, L. Montanaro, C. R. Arciola, *Biomaterials* **2013**, *34*, 8533.
[18] M. A. Cook, G. D. Wright, *Sci. Transl. Med.* **2022**, *14*, 7793.
[19] N. Y. Lee, W. C. Ko, P. R. Hsueh, *Front. Pharmacol.* **2019**, *10*, 1.
[20] M. Riool, A. de Breij, L. de Boer, P. H. S. Kwakman, R. A. Cordfunke, O. Cohen, N. Malanovic, N. Emanuel, K. Lohner, J. W. Drijfhout, P. H. Nibbering, S. A. J. Zaat, *Adv. Funct. Mater.* **2017**, *27*, 201606623.
[21] A. de Breij, M. Riool, R. A. Cordfunke, N. Malanovic, L. de Boer, R. I. Koning, E. Ravensbergen, M. Franken, T. van der Heijde, B. K. Boekema, P. H. S. Kwakman, N. Kamp, A. El Ghalbzouri, K. Lohner, S. A. J. Zaat, J. W. Drijfhout, P. H. Nibbering, *Sci. Transl. Med.* **2018**, *10*, aan4044.
[22] W. Song, J. Zhang, J. Guo, J. Zhang, F. Ding, L. Li, Z. Sun, *Toxicol. Lett.* **2010**, *199*, 389.
[23] A. D. L. Rodríguez López, M. R. Lee, B. J. Ortiz, B. D. Gastfriend, R. Whitehead, D. M. Lynn, S. P. Palecek, *Acta Biomater.* **2019**, *93*, 50.
[24] Y. Lyu, Y. Yang, X. Lyu, N. Dong, A. Shan, *Sci. Rep.* **2016**, *6*, 1.
[25] B. Costa, G. Mart, P. A. C. Gomes, M. C. L. Martins, *Pharmaceutics* **2021**, *13*, 1.
[26] H. Scheper, J. M. Wubbolts, J. A. M. Verhagen, A. W. de Visser, R. J. P. van der Wal, L. G. Visser, M. G. J. de Boer, P. H. Nibbering, *Front. Microbiol.* **2021**, *12*, 1.
[27] S. Amin Yavari, S. M. Castenmiller, J. A. G. van Strijp, M. Croes, *Adv. Mater.* **2020**, *32*, 1.
[28] S. C. Mansour, O. M. Pena, R. E. W. Hancock, *Trends Immunol.* **2014**, *35*, 443.
[29] U. H. N. Dürr, U. S. Sudheendra, A. Ramamoorthy, *Biochim. Biophys. Acta – Biomembr.* **2006**, *1758*, 1408.
[30] M. Bacalum, M. Radu, *Int. J. Pept. Res. Ther.* **2015**, *21*, 47.
[31] C. H. Enoksen, T. S. Wik, J. Klaksvik, J. Astvaldur, *J. Eng. Med.* **2017**, *231*, 1195.
[32] International Organization for Standardization. (2009). *Biological evaluation of medical devices* (ISO Standard No. 10993-5:2009(E)).
[33] C. D. Ciornei, T. Sigurdardóttir, A. Schmidtchen, M. Bodelsson, *Antimicrob. Agents Chemother.* **2005**, *49*, 2845.
[34] A. Panáček, L. Kvítek, M. Smékalová, R. Vecerová, M. Kolar, M. Röderová, F. Dycka, M. Sebela, R. Prucek, O. Tomanec, R. Zboril, *Nat. Nanotechnol.* **2018**, *13*, 65.
[35] N. Niño-Martínez, M. F. Salas Orozco, G. A. Martínez-Castañón, F. T. Méndez, F. Ruiz, *Int. J. Mol. Sci.* **2019**, *20*, 2808.
[36] S. J. Pidot, W. Gao, A. H. Buultjens, I. R. Monk, R. Guerillot, G. P. Carter, J. Y. H. Lee, M. M. C. Lam, M. L Grayson, S. A. Ballard, A. A. Mahony, E. A. Grabsch, D. Kotsanas, T. M. Korman, G. W. Coombs, J. O Robinson, A. Gonçalves da Silva, T. Seemann, B. P. Howden, P. D. R. Johnson, T. P. Stinear, *Sci. Transl. Med.* **2018**, *10*.
[37] J. M. Damerau, S. Bierbaum, D. Wiedemeier, P. Korn, R. Smeets, G. Jenny, J. Nadalini, B. Stadlinger, *J. Biomed. Mater. R es.* **2022**, *110*, 157.

[38] B. Wu, Y. Tang, K. Wang, X. Zhou, L. Xiang, *Int. J. Nanomed.* **2022**, *17*, 1865.
[39] G. Zhu, G. Wang, *Mater. Adv.* **2021**, *2*, 6901.
[40] G. I. l. Im, *Biomater. Res.* **2020**, *24*, 7.
[41] B. Herrero de la Parte, I. Rodrigo, J. Gutierrez-Basoa, S. Iturrizaga Correcher, *Cancers* **2022**, *14*, 1.
[42] B. Kozissnik, A. C. Bohorquez, J. Dobson, C. Rinaldi, *Int. J. Hyperth.* **2013**, *29*, 706.
[43] X. Du, M. Zhang, H. Zhou, W. Wang, C. Zhang, L. Zhang, Y. Qu, W. Li, X. Liu, M. Zhao, K. Tu, Y.-Q. Li, *Research* **2022**, *2022*, 1.
[44] S. Rotundo, D. Brizi, A. Monorchio, *Sensors* **2022**, *22*, 5132.
[45] B. Jia, X. Du, W. Wang, Y. Qu, X. Liu, M. Zhao, W. Li, Y.-Q. Li, *Adv. Sci.* **2022**, *9*, 1.
[46] B. Sanz, M. P. Calatayud, T. E. Torres, M. R. Ibarra, G. F. Goya, *Biomaterials* **2017**, *114*, 62.
[47] J. Xu, S. Zhang, A. Machado, S. Lecommandoux, O. Sandre, *Sci. Rep.* **2017**, *7*, 1.
[48] C. Yuan, S. Jin, J. Wei, J. Huang, C. Liu, X. Lei, Y. Zuo, J. Li, Y. Li, *J. Mater. Chem. B* **2021**, *9*, 5861.
[49] A. Zeb, M. Gul, T.-T.-L. Nguyen, H.-J. Maeng, *J. Pharm. Investig.* **2022**, *52*, 683.
[50] A. I. Visan, G. Popescu-pelin, G. Socol, *Polymers* **2021**, *13*, 1.
[51] A. D. Padsalgikar, in *4 Biological Properties of Plastics. in Plastics in Medical Devices for Cardiovascular Applications*, Elsevier, Amsterdam, **2017**, pp 83–102.
[52] C. D'Avila Carvalho Erbetta, R. J. Alves, J. Resende Magalhães, F. de Souza Freitas, R. G. de Sousa, *J. Biomater. Nanobiotechnol.* **2012**, *3*, 208.
[53] International Organization for Standardization. (1989). *General tolerances – Part 1: Tolerances for linear and angular dimensions without individual tolerance indications* (ISO Standard No. 2768-1:1989(E)).
[54] C. Kuo, C. Su, A. Chiang, *Int. J. Precis. Eng. Manuf.* **2017**, *18*, 1609.
[55] A. H. Maamoun, Y. F. Xue, M. A. Elbestawi, S. C. Veldhuis, *Materials* **2018**, *11*, 2343.
[56] D. Soler, M. Telleria, P. J. Arrazola, *J. Manuf. Mater. Process.* **2022**, *6*, 82.
[57] M. Wang, Y. Wu, S. Lu, T. Chen, Y. Zhao, H. Chen, Z. Tang, *Prog. Nat. Sci.: Mater. Int.* **2016**, *26*, 671.
[58] I. Koutiri, E. Pessard, P. Peyre, O. Amlou, T. De Terris, *J. Mater. Process. Technol.* **2018**, *255*, 536.
[59] A. Majeed, A. Ahmed, A. Salam, M. Z. Sheikh, *Int. J. Light. Mater. Manuf.* **2019**, *2*, 288.
[60] A. B. Faia-Torres, M. Charnley, T. Goren, S. Guimond-Lischer, M. Rottmar, K. Maniura-Weber, N. D. Spencer, R. L. Reis, M. Textor, N. M. Neves, *Acta Biomater.* **2015**, *28*, 64.
[61] B. D. Boyan, E. M. Lotz, Z. Schwartz, *Tissue Eng., Part A* **2017**, *23*, 1479.
[62] T. Zakrzewski, J. Kozak, M. Witt, M. Debowska-Wasak, *Proc. CIRP* **2020**, *95*, 115.
[63] B. Nagarajan, Z. Hu, X. Song, W. Zhai, J. Wei, *Engineering* **2019**, *5*, 702.
[64] N. Mookherjee, M. A. Anderson, H. P. Haagsman, D. J. Davidson, *Nat. Rev. Drug Discovery* **2020**, *19*, 311.
[65] M. Mahlapuu, A. Sidorowicz, J. Mikosinski, M. Dyaczynski, B. B. G. Dziwiszek, *Wound Repair Regen.* **2021**, *29*, 938.
[66] M. R. Scheenstra, M. van den Belt, J. L. M. Tjeerdsma-van Bokhoven, V. A. F. Schneider, S. R. Ordonez, A. van Dijk, E. J. A. Veldhuizen, H. P. Haagsman, *Sci. Rep.* **2019**, *9*, 1.
[67] J. Johansson, G. H. Gudmundsson, M. E. Rottenberg, K. D. Berndt, B. Agerberth, *J. Biol. Chem.* **1998**, *273*, 3718.
[68] E. Anders, S. Dahl, D. Svensson, B. O. Nilsson, *Biochem. Biophys. Res. Commun.* **2018**, *501*, 280.
[69] J. Säll, M. Carlsson, O. Gidlöf, A. Holm, J. Humlén, J. Öhman, D. Svensson, B. O. Nilsson, D. Jönsson, *J. Innate Immun.* **2013**, *5*, 290.
[70] E. Bankell, S. Dahl, O. Gidlöf, D. Svensson, B. O. Nilsson, *Peptides* **2021**, *135*, 15.
[71] A. M. van der Does, H. Beekhuizen, B. Ravensbergen, T. Vos, T. H. M. Ottenhoff, J. T. van Dissel, J. W. Drijfhout, P. S. Hiemstra, P. H. Nibbering, *J. Immunol.* **2010**, *185*, 1442.
[72] M. G. Scott, D. J. Davidson, M. R. Gold, D. Bowdish, R. E. W. Hancock, *J. Immunol.* **2002**, *169*, 3883.
[73] X. Yu, J. Quan, W. Long, H. Chen, R. Wang, J. Guo, X. Lin, S. Mai, *Exp. Cell Res.* **2018**, *372*, 178.
[74] L. Li, Y. Peng, Q. Yuan, J. Sun, A. Zhuang, X. Bi, *Front. Bioeng. Biotechnol.* **2021**, *9*, 1.
[75] Z. Chinipardaz, J. M. Zhong, S. Yang, *Life* **2022**, *12*, 1.
[76] X. Shen, M. A. Al-Baadani, H. He, L. Cai, Z. Wu, L. Yao, X. Wu, S. Wu, M. Chen, H. Zhang, J. Liu, *Int. J. Nanomed.* **2019**, *14*, 3043.
[77] K. G. Choi, S. Napper, *Immunology* **2014**, *143*, 68.
[78] M. E. van Gent, T. J. K. van der Reijden, P. R. Lennard, A. W. de Visser, B. Schonkeren-Ravensbergen, N. Dolezal, R. A. Cordfunke, J. W. Drijfhout, P. H. Nibbering, *Antibiotics* **2022**, *11*, 673.
[79] G. S. Dijksteel, M. M. W. Ulrich, P. H. Nibbering, R. A. Cordfunke, J. W. Drijfhout, E. Middelkoop, B. K. H. L. Boekema, *J. Microbiol. Antimicrob.* **2020**, *12*, 70.
[80] H. Li, S. Zhang, B.' Nie, Z. Du, T. Long, B. Yue, *RSC Adv.* **2018**, *8*, 15547.
[81] P. G. Lima, J. T. A. Oliveira, J. L. Amaral, C. D. T. Freitas, P. F. N. Souza, *Life Sci.* **2021**, *278*, 119647.